Fibril Formation in *In Situ* Composites of a Thermotropic Liquid Crystalline Polymer in a Thermoplastic Matrix

G. CREVECOEUR* and G. GROENINCKX†

Department of Chemistry, Laboratory for Macromolecular Structural Chemistry, Catholic University of Leuven, Celestijnenlaan 200 F, 3001 Heverlee, Belgium

SYNOPSIS

Blends of a thermotropic liquid crystalline polymer, Vectra B950, and a matrix of poly(phenylene ether) and polystyrene were extruded through a capillary designed to yield a converging flow with a constant elongational rate of strain. Fibril formation of the Vectra phase, initially dispersed as spherical droplets, was studied as a function of strain rate and blend composition. It was found that for blends with low Vectra contents, i.e., small Vectra particles, or below a minimum strain rate, no fibril formation takes place. These phenomena could be explained by the balance between interfacial tension and shear stress in the flow field. The critical conditions for fibril formation, estimated from these experiments, are comparable to the literature data. Furthermore, the elongational viscosity of the blends was calculated from the pressure gradient over the capillary. The elongational viscosity was found to decrease with Vectra content, to observe power-law behavior, and to be three orders of magnitude larger than the shear viscosity of the blends. © 1993 John Wiley & Sons, Inc.

INTRODUCTION

In situ composites of a thermotropic liquid crystalline polymer (TLCP) in a thermoplastic matrix, first introduced by Kiss,[1] have received considerable interest in the literature over the past few years and a number of reviews have recently been published.[2-7] The processing of *in situ* composites involves two essential steps: The first is the dispersion of the TLCP in the thermoplastic matrix as fine (usually spherical) droplets, e.g., in a twin-screw extruder or in a static mixer. The second step is the extension of these drops into fibrils with a high aspect ratio in a strong, preferably elongational, flow field, e.g., in the die of the extruder or by melt drawing/spinning. As the mechanical properties, in particular the tensile modulus, of *in situ* composites strongly depend on the aspect ratio of the TLCP fibrils, the process of fiber formation is of paramount importance to the final performance of the *in situ* composite. Numerous studies have been devoted to the relation between processing conditions and the resulting morphology of *in situ* composites; nevertheless, there is still a lack of basic understanding of the parameters that determine the desired fibril formation. In some cases, it is found, for instance, that a certain minimum TLCP content (10–30 wt %, depending on the blend components and the processing conditions) is required for fibril formation.[8-12] As will be shown below, such phenomena may, at least qualitatively, be explained by classical microrheology of multiphase flows.

In this paper, the deformation behavior of TLCP droplets in a thermoplastic matrix is investigated, using a capillary designed to yield an elongational flow with a constant strain rate. Previous experiments have pointed out that elongational flows (so-called strong flows) are much more effective than are shear flows (weak flows) in elongating dispersed TLCP droplets into fine reinforcing fibrils.[13] The blend components for this study are the commercial TLCP Vectra B950 and a matrix consisting of 70 wt % poly(phenylene ether) and 30 wt % polystyrene [PPE/PS (70/30)]. Since PPE and PS are

* Present address: DSM Research, Department for Polymeric Construction Materials, P.O. Box 18, 6160 MD Geleen, The Netherlands.

† To whom correspondence should be addressed.

Journal of Applied Polymer Science, Vol. 49, 839–849 (1993)
 CCC 0021-8995/93/050839-11

miscible over the entire composition range, the blends are in all cases two-phase systems of the PPE/PS matrix and the TLCP, which is immiscible with the matrix. The processing, morphology, and mechanical behavior of Vectra B950-PPE/PS (70/30) *in situ* composites have comprehensively been studied in our laboratory.[13-16]

THEORY: MICRORHEOLOGY OF MULTIPHASE FLOWS

The initial stages of mixing of two polymers, where the size of the minor component is still large, are governed by the amount of interface created, which is proportional to the total shear γ applied. The amount of interface created strongly depends on the number of reorientations, introducing an exponential increase with γ.[17] During mixing, the extended particles continuously decrease in diameter and the interfacial stress[‡] increases progressively and will finally be of the same order of magnitude as of the shear stress $\tau = \eta_c\dot{\gamma}$ applied (with η_c the viscosity of the continuous phase and $\dot{\gamma}$ the shear rate). Dispersive mixing starts with the growth of distortions on the long slender bodies that are formed. Interfacial tension-driven Rayleigh disturbances eventually lead to disintegration of the threads into a series of small droplets.[17,18] These droplets may be deformed again and break up into even smaller droplets, until the shear stress τ is counterbalanced by the interfacial stress, σ/R, that resists the deformation. Therefore, the ratio between shear stress and interfacial tension, as expressed in the dimensionless capillary number Ca:

$$Ca = \frac{\tau R}{\sigma} = \frac{\eta_c\dot{\gamma}R}{\sigma} \qquad (1)$$

determines the final equilibrium size of an isolated droplet in a given flow field. Below a certain critical value of Ca, Ca_{crit}, the interfacial forces withstand the flow field, and no sufficient deformation can take place to lead to further breakup. Hence, Ca_{crit} determines the smallest possible particle size that can be obtained. Ca_{crit} is strongly dependent on the type of flow and the viscosity ratio $p = \eta_d/\eta_c$ of the dispersed and continuous phases. This type of flow can be simple shear flow, like the rotational Couette flow, or irrotational shear flow, as present in elongational flows. Experimental relations between Ca_{crit} and the viscosity ratio have been obtained for Newtonian model fluids[19] and also for polymer melts[20]; they indicate that the dispersive process becomes increasingly difficult for viscosity ratios deviating from 1.

The dispersive mixing process describes the deformation of an isolated droplet and determines the smallest obtainable particle size. The mean particle size in the blend, however, is the result of a dynamic equilibrium between dispersive mixing and coalescence of droplets. The number of particles increases dramatically with the volume fraction of the dispersed phase and so does the collision probability of particles in the melt. As a consequence, the average particle size increases with increasing volume fraction of the dispersed phase, until somewhere around the 50/50 composition (depending on viscosity ratio) the morphology becomes co-continuous. Because the TLCP in *in situ* composites is initially dispersed as droplets that are subsequently elongated in a flow field, the TLCP content is expected to have influence on the final composite morphology. Elemans and Janssen[17,21] found that for Newtonian fluids in a simple shear flow field, with $Ca > 2Ca_{crit}$, an isolated droplet deforms affinely with the macroscopic flow. The combined processes of breakup and coalescence is still not very well understood and no quantitative theory exists. Nevertheless, qualitatively it can be expected that in blends with a high TLCP content, with large droplets due to coalescence, the TLCP drops will undergo affine deformation. For the lower TLCP content blends, however, Ca may become of the same order of magnitude as Ca_{crit} and the deformation may be less than affine. This would result in TLCP fibrils with lower aspect ratio and/or lower molecular orientation within the TLCP, as the latter (for pure TLCPs) is known to depend on total shear, but not on shear rate.[22,23]

EXPERIMENTAL

The Capillary and Elongational Viscosity Measurements

A special "trumpet-die" was designed for elongational viscosity measurements. The design equations for this capillary relating the throughput Q to the strain rate $\dot{\varepsilon}$, are described in the Appendix. The elongational viscosity of the blends may be estimated from the pressure gradient over this capillary. This pressure difference basically contains three contributions[24,25]: a contribution due to the elon-

[‡] For the geometry of a droplet in a flow field, the interfacial stress is σ/R, with σ the interfacial tension and R the radius of the droplet.

gational stress ΔP_e, from which the elongational viscosity may be obtained; a contribution from the shear stress at the wall ΔP_s; and an elastic contribution that is correlated to the first normal stress difference. As the first normal stress difference is experimentally difficult to assess, and TLCPs are generally known to produce low normal stresses, e.g., Ref. 26, the latter is ignored in a first approximation. The influence of the shear contribution will be considered in more detail. It is demonstrated in the Appendix that for a power-law fluid with

$$\eta = \eta_0 \dot{\gamma}^{n-1} \tag{2}$$

and assuming a fully developed velocity profile in every cross section of the capillary, the shear contribution to the pressure drop over the capillary is given by

$$\Delta P_s = \left[2\eta_0 \left(\frac{1+3n}{n} \frac{Q}{\pi} \right)^n \left(\frac{2Q}{\pi \dot{\epsilon}(3n+3)} \right) \right] \times \left[\left(\frac{1}{R_1^2} \right)^{(3n+3)/2} - \left(\frac{1}{R_0^2} \right)^{(3n+3)/2} \right] \tag{3}$$

with $\dot{\epsilon}$ the (elongational) strain rate, Q the throughput, and R_0 and R_1 the radius of the capillary at the entrance and exit, respectively. Thus, the shear contribution to the pressure difference can be calculated from the shape of the capillary and the plunger speed if the viscosity of the melt, in terms of its power-law constants, is known. From the corrected pressure difference ($\Delta P_e = \Delta P_t - \Delta P_s$), the elongational viscosity may be estimated:

$$\Delta P_e = \frac{2\eta_e Q}{\pi L} \left[\ln \left(\frac{R_0}{R_1} \right) \right] \left(\frac{1}{R_1^2} - \frac{1}{R_0^2} \right) \tag{4}$$

with η_e the elongational viscosity and L the length of the capillary (see Appendix). It is interesting to note the resemblance of eq. (4) to Cogswell's equation for a coni-cylindrical die[25], which can be written as

$$\Delta P_e = \frac{2\eta_e Q}{\pi L} \cdot 2(R_0 - R_1) \cdot \left(\frac{1}{R_1^3} - \frac{1}{R_0^3} \right) \tag{5}$$

Materials, Blend Preparation, and Capillary Experiments

PPE/PS (70/30) blends were supplied by General Electric Plastics Europe and Vectra B950 was purchased from Hoechst Celanese; the materials were used as received after drying. Blends with different compositions were compounded on a Berstorff ZE 25 corotating twin-screw extruder with L/D of 33, operating at 250 rpm at a throughput of 5 kg/h and with a barrel temperature of 300°C. The extrudate was water-quenched and pelletized and, after drying, used for experiments in the capillary rheometer.

The temperature of the rheometer was set at 300°C, and the plunger speed was varied from 0.1 to 5 mm s^{-1}, corresponding to strain rates from 0.084 to 4.2 s^{-1}. Before capillary extrusion, the material was allowed to melt in the reservoir for 5 min. The strands were directly quenched in a water bath to preserve the morphology for further characterization. During the experiments, the pressure, measured just above the entrance of the capillary, was recorded.

Characterization of the Strands

Scanning electron microscopy (SEM) was used to study the morphology of the strands from the capillary rheometer. Fracture surfaces, perpendicular to the processing direction, were obtained by breaking the strands at cryogenic temperature and gluing them on the sample holder using conductive carbon cement. The samples were coated with a gold layer of approximately 30 nm and examined in a Philips SEM at an accelerating voltage of 25 kV.

Molecular orientation of the TLCP fibrils in the strands was assessed using wide-angle X-ray scattering (WAXS). Two-dimensional diffraction patterns were recorded on flat film in a Kiessig camera using a point collimated X-ray beam from a CuKα source. The camera was kept under vacuum during exposure to minimize air-scattering. The scattering patterns of the blends were composed of the sharp equatorial 110 reflection of the TLCP superimposed on an amorphous halo originating from the PPE/PS matrix. This amorphous halo did not show any appreciable orientation in the drawing direction, and the intensity was equally distributed over the entire circular range. Furthermore, it had its maximum at a lower diffraction angle than that of the Vectra reflection, so that these two reflections did not interfere for blends containing 25 wt % or more Vectra B950. To quantify the molecular orientation, an azimuthal densitometer-scan over the equatorial TLCP reflection was made, and the molecular orientation was expressed as the second moment of the orientation distribution (or Hermans orientation factor) P_2, which is defined as[27,28]:

$$P_2 = \frac{3\langle \cos^2 \Phi \rangle - 1}{2} \tag{6}$$

where $\langle \cos^2 \Phi \rangle$ is an integrated intensity-average over all azimuthal angles. Note that the formalism used for the calculation of P_2 assumes that the TLCP molecules are perfectly oriented within domains and that the value of P_2 is determined by the degree of misalignment between these domains.

Shear Viscosity Measurements

Shear viscosity as a function of shear rate of the PPE/PS (70/30)–Vectra B950 blends at 300°C was measured in steady shear deformation on a Physica MC 20 rheometer. The measurements were performed in cone-plate geometry, using a cone with a diameter of 25 mm and a top angle of 2°. The temperature was controlled by a flow of electrically heated nitrogen, of more than 100 L per min, around the cone and plate. Nitrogen was used to minimize oxidation reactions during the measurements. Viscosity curves were obtained in a controlled shear stress mode.

RESULTS AND DISCUSSION

Morphology

The morphology of the extruded strands containing 1–25 wt % TLCP is depicted in the micrographs in Figure 1 as a function of the strain rate. Note that the horizontal axis is logarithmic for the strain rate (relating to the available plunger speeds on the capillary rheometer) and that the vertical axis does not scale particularly with the blend composition or any particle size. A number of observations can be made from this figure.[§] First of all, it is clearly seen that the particle size of the TLCP dispersed phase increases with the TLCP content, in agreement with the increased chance of coalescence as discussed above. For the 1 wt % TLCP sample, containing the smallest TLCP particles, the TLCP is dispersed as spherical droplets over the entire shear rate range covered in this experiment. Apparently, the capillary number in elongational flow, Ca, was below its critical value Ca_{crit} and the shear forces could not overcome the interfacial tension, so that no deformation took place. For the 5 wt % TLCP sample, a transition from spherical to fibrillar particles is observed in the strain rate range from 0.42 to 0.84 s^{-1}. Since the initial TLCP droplets are larger here, the effect of the interfacial tension is smaller and the capillary number is apparently of the order of its critical value. A similar transition is observed for the 10 wt % TLCP blends, but at a somewhat lower shear rate (0.17–0.42 s^{-1}). For the even larger particles in the 25 wt % TLCP blend, the transition from droplets to fibrils already takes place at the lowest strain rate that was measured.

These findings illustrate that elongation of TLCP particles into fibrils qualitatively fits the above discussed microrheological principles for multiphase flows; below a minimum strain rate or minimum particle size, no fibril formation seems to take place. Although the explanation seems reasonable, it should be emphasized that implicitly two assumptions are made with respect to the influence of time effects and the quenching of the strands: It is assumed here that for the low strain rates, where the TLCP droplets were not or only slightly deformed (i.e., $Ca \ll Ca_{crit}$), the time of flow through the trumpet die was sufficient for an equilibrium deformation of the TLCP droplets to take place and that the quenching in the water bath immediately below the die was fast enough to prevent any breakup or relaxations of the fibrils. The observed deformation behavior of the TLCP particles also implies that fibril formation is not unique to TLCP–thermoplastic systems. Indeed, Vinogradov et al.[29,30] and Tsebrenko[31] comprehensively studied the conditions for fibril formation in thermoplastic model systems. The advantage, however, of applying this technique to TLCP–thermoplastic systems is the easy orientation of TLCPs and their corresponding favorable mechanical properties. For this reason, the molecular orientation, closely related to both the total deformation of a TLCP droplet and its resulting mechanical properties, was studied for the above samples.

Molecular Orientation

The Hermans orientation factor P_2 for blends containing 25, 50, and 100 wt % Vectra B950 is plotted vs. strain rate in Figure 2. The molecular orientation could not be determined for any lower TLCP content

[§] In the following discussion, it is implicitly assumed that the TLCP is initially, i.e., before being subjected to the elongational deformation imposed by the flow field, dispersed as spherical droplets. In some cases,[13] the granules, as obtained from the primary compounding step that are used for the experiments, may contain TLCP fibrils. Compression-molding experiments with the Vectra B950–PPE/PS (70/30) blends have shown, however, that within times of 8–10 min, comparable to the 5 min heating time used in the current experiments, this fibrillar morphology was completely erased and only spherical droplets in a matrix were found. The assumption that the TLCP particles were all spherical prior to extrusion through the trumpet die seems therefore reasonable. This is further substantiated by the micrographs of the samples with the lowest TLCP content, where no deformation of the TLCP took place, and the spherical particles found after capillary extrusion thus reflect the initial morphology.

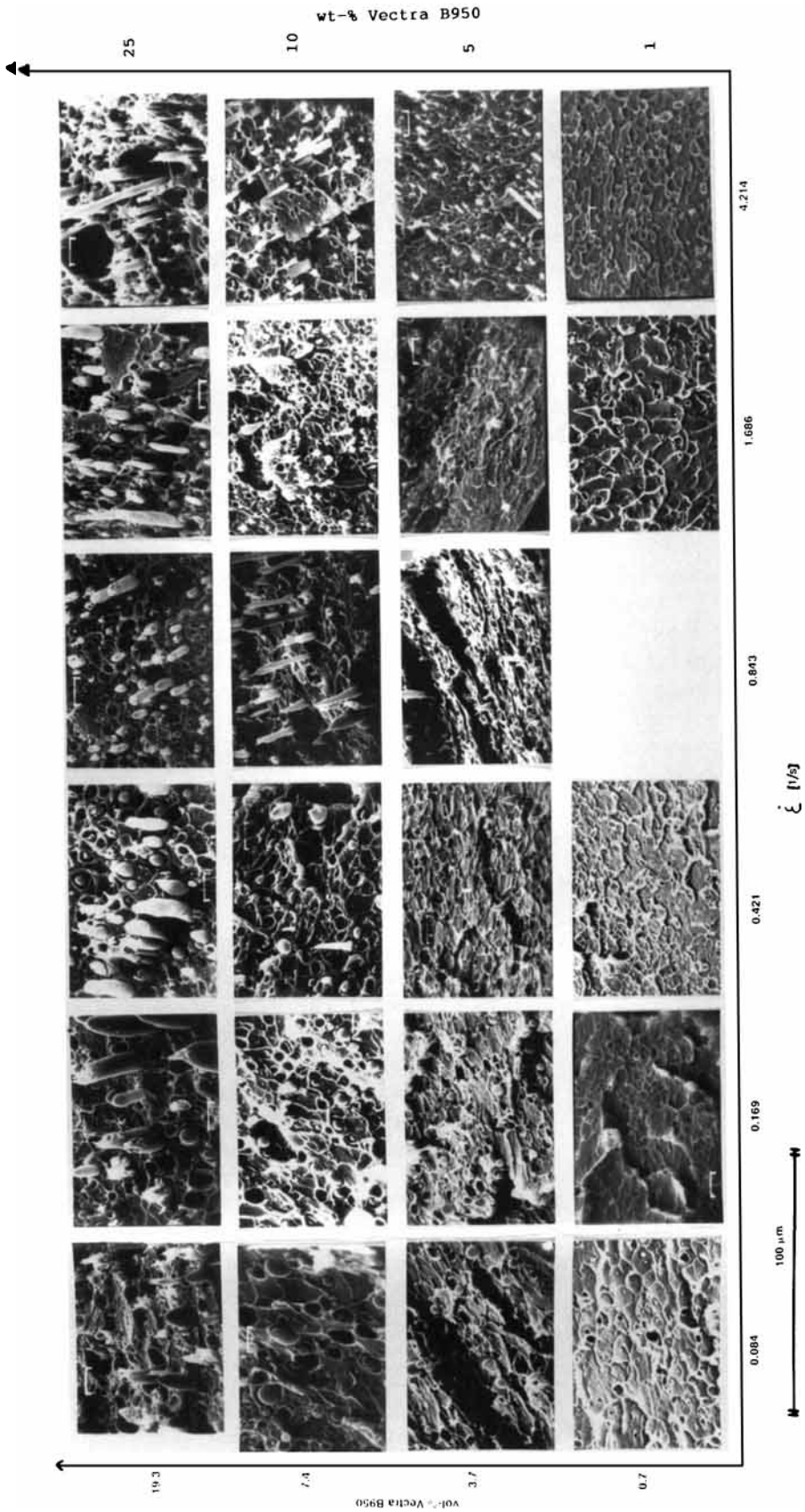

Figure 1 Scanning electron micrographs of PPE/PS (70/30)–Vectra B950 strands, extruded through a capillary with constant strain rate. Strain rate on horizontal axis; composition on vertical axis.

composition, since the intensity of the equatorial 110 reflection of Vectra B950 was too low compared to the amorphous background halo of the PPE/PS (70/30) matrix.

Figure 2 reveals that molecular orientation does not change appreciably with strain rate, at least not within the experimental accuracy. Obviously, for these compositions, the ratio of Ca/Ca_{crit} is much larger than for the low TLCP content blends depicted in Figure 1 and may be considered to be well above its critical value. Thus, the deformation of the TLCP droplets would be more or less affine with the macroscopic flow field and, therefore, show no dependence on the deformation rate, but only on the total deformation that was constant for all experiments. In contrast to this, however, there is a pronounced influence of composition on molecular orientation, which is seen to increase with TLCP content. A similar increase in molecular orientation with TLCP content was found for lower TLCP contents in our previous studies on the system PPE/PS (70/30)–Vectra B950[13,15,16] as well as in others.[12,32-36] The increase in molecular orientation found here indicates that even for the high TLCP contents the deformation is not yet entirely affine with the flow field, since in that case, molecular orientation would have been independent of composition. At this stage, the authors have no explanation for this surprising behavior.

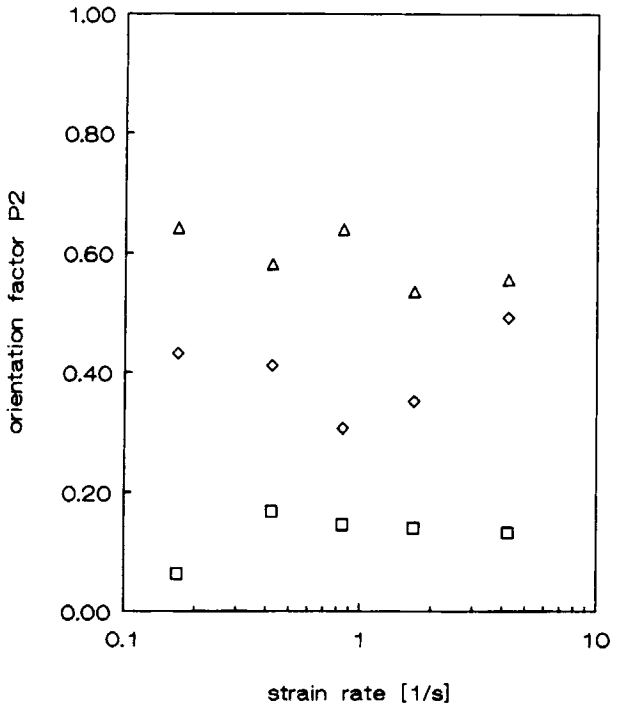

Figure 2 Hermans orientation factor for PPE/PS (70/30)–Vectra B950 blends containing (□) 25, (◇) 50, and (△) 100 wt % Vectra B950 vs. strain rate.

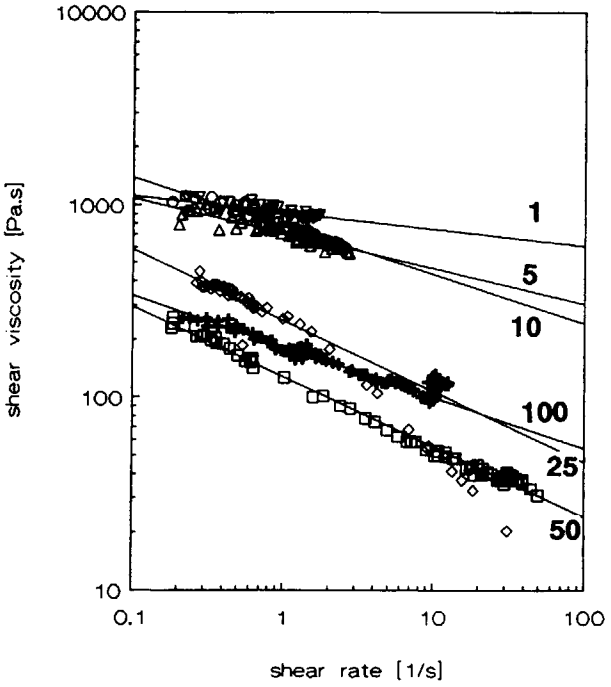

Figure 3 Plot of shear-rate dependency of viscosity of PPE/PS (70/30)–Vectra B950 blends at 300°C · wt % Vectra B950 indicated in the figure.

Shear and Elongational Viscosities

The shear viscosity of the PPE/PS (70/30)–Vectra B950 blends is plotted vs. shear rate in Figure 3. All compositions are seen to exhibit a more or less power-law behavior, and, basically, the viscosity decreases with TLCP content, as would be expected, although not monotonously. Remarkably, the viscosity of pure Vectra B950 is higher than that of the 50 wt % Vectra B950 blend. Surprising viscosity–composition behavior, with intermediate minima and maxima, has been observed before.[37-41] It should be noted, however, that there were some difficulties in the viscosity measurements due to degradation of the PPE/PS (70/30) matrix at these high temperatures and some flow instability of Vectra B950. Nevertheless, these data give at least an indication of the magnitude of the viscosity and, thus, are used in the calculations of the elongational viscosity.[‖] All

[‖] Note that using the shear viscosity data for flow calculations through the capillary involves only a moderate extrapolation of the flow curves. The shear rate at the end of the capillary (where it is maximal) was estimated to be 8.5 s^{-1} for the lowest plunger speed and 425 s^{-1} for the highest plunger speed. It is also seen in Table I that ΔP_s constitutes only a small part of the total pressure difference, and, therefore, the influence of the shear data on the elongational viscosity is small.

Table I Shear and Elongational Viscosity Data for PPE/PS (70/30)–Vectra B950 Blends

Wt % Vectra B950	η_0 (Pas)	n	Plunger Speed (mms^{-1})	$\dot{\varepsilon}$ (s^{-1})	ΔP_t (bar)	ΔP_s (bar)	ΔP_e (bar)	η_e (MPas)
1	913.1	0.913	0.1	0.084	25	1.85	23.14	5.94
			0.2	0.169	50	3.49	46.52	5.97
			0.5	0.421	90	8.05	81.95	4.21
			1.0	0.843	130	15.15	114.84	2.95
			2.0	1.686	175	28.53	146.47	1.88
			5.0	4.214	275	65.83	209.17	1.074
5	711.1	0.816	0.1	0.084	20	1.24	18.76	4.82
			0.2	0.169	45	2.17	42.82	5.50
			0.5	0.421	45	4.59	40.41	2.07
			1.0	0.843	10	8.09	91.91	2.36
			2.0	1.686	135	14.24	120.76	1.55
			5.0	4.214	205	30.08	174.92	0.90
10	776.3	0.747	0.1	0.084	25	1.21	23.79	6.11
			0.2	0.169	35	2.03	32.97	4.23
			0.5	0.421	60	4.02	55.98	2.87
			1.0	0.843	80	6.74	73.26	1.88
			2.0	1.686	110	11.31	98.69	1.27
			5.0	4.214	170	22.41	147.59	0.76
25	251.0	0.632	0.1	0.084	15	0.33	14.67	3.77
			0.2	0.169	25	0.50	24.50	3.14
			0.5	0.421	38	0.90	37.10	1.90
			1.0	0.843	55	1.39	53.61	1.38
			2.0	1.686	75	2.16	72.84	0.93
			5.0	4.214	120	3.85	116.15	0.60
50	128.3	0.635	0.1	0.084	1.5	0.17	1.33	0.34
			0.2	0.169	3	0.26	2.74	0.35
			0.5	0.421	15	0.47	14.53	0.75
			1.0	0.843	30	0.72	29.28	0.75
			2.0	1.686	45	1.12	43.88	0.56
			5.0	4.214	90	2.01	87.99	0.45
100	183.7	0.735	0.1	0.084	0	—	—	—
			0.2	0.169	0	—	—	—
			0.5	0.421	5	0.92	4.08	0.21
			1.0	0.843	15	1.52	13.48	0.35
			2.0	0.1686	25	2.54	22.46	0.29
			5.0	4.214	50	4.98	45.02	0.23

Shear data from rotational shear tests and elongational data from capillary rheometer tests (see text). Temperature for all experiments 300°C.

data were fitted to the power-law equation [eq. (2)], and the zero-shear viscosity and power-law coefficient are given in Table I.

The shear contribution to the pressure drop over the capillary was calculated according to eq. (3) and the results are listed in Table I. ΔP_s is seen to be no more than 10–20% of the total pressure difference. From the corrected pressure difference ΔP_e, the elongational viscosity of the blends was calculated using eq. (4) and is given in Table I and Figure 4. The values are substantially higher (three orders of magnitude) than those for the shear viscosity. (Note that the data in Table I and Figure 4 are given in MPas.) The averaged elongational viscosity shows a clear power-law behavior and decreases monotonously with increasing TLCP content. Zero-shear elongational viscosities and power-law coefficients (denoted m for distinction from the shear power-law coefficient) are given in Table II. Elongational viscosities of Vectra A950, polycarbonate, and a

20/80 blend of these components, measured with a converging capillary using the Cogswell method, were recently reported by Beery et al.[42] They also found high values for the elongational viscosity, between 0.01 and 10 MPas, but, interestingly, they found an increase in elongational viscosity with increasing TLCP content.

Estimation of the Critical Capillary Number

As has been demonstrated in the previous sections that the elongation of TLCP droplets into fibrils is quite comparable to the microrheology of conventional polymer blends, it is interesting to estimate the critical capillary number for deformation in elongational flow from the above data. It is emphasized that the critical capillary number is rather freely interpreted here as the transition from spherical droplets, i.e., no deformation of the TLCP particles, to ellipsoidal or fibrillar, i.e., deformed, TLCP particles. Figure 1 provides the average particle size of droplets that are just too small to be deformed, i.e., $Ca \approx Ca_{crit}$; these were estimated as

3 μm for the 5 wt % Vectra B950 blend, at $\dot{\varepsilon} = 0.169\ s^{-1}$;

6 μm for the 10 wt % Vectra B950 blend, at $\dot{\varepsilon} = 0.084\ s^{-1}$.

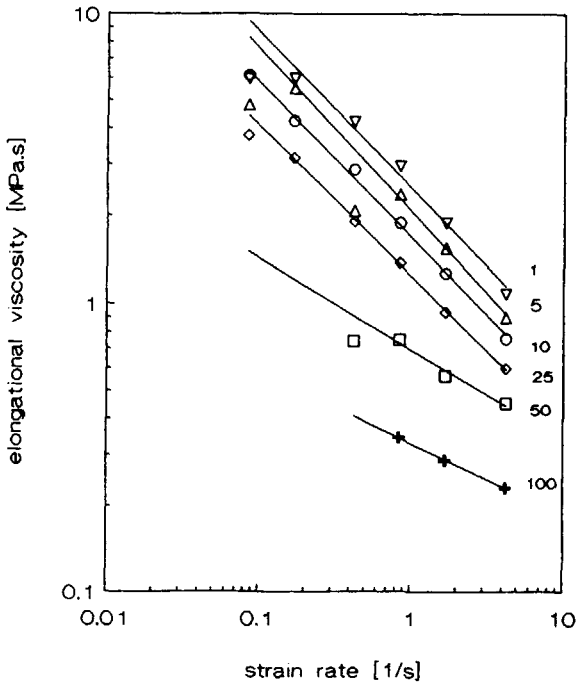

Figure 4 Plot of strain-rate dependency of elongational viscosity of PPE/PS (70/30)–Vectra B950 blends at 300°C · wt % Vectra B950 indicated in the figure.

Table II Zero-strain Elongational Viscosity and Power-Law Coefficient for PPE/PS (70/30)–Vectra B950 Blends at 300°C

Wt % Vectra B950	$\eta_{e,0}$ (MPas)	m
1	2.48	0.46
5	2.06	0.44
10	1.68	0.47
25	1.24	0.48
50	0.69	0.69
100	0.33	0.75

Thus, R and $\dot{\varepsilon}$ are known. The shear rate, $\dot{\gamma}$, to be used in the calculation of the capillary number [eq. (1)] according to its original definition for a 2-D plane elongational flow (Couette or four-roll mill),[43–46] equals $\sqrt{3}\dot{\varepsilon}$ for the geometry used in the present experiments.[47] The stresses that the matrix acts on the TLCP droplet are shear stresses, and for this reason, the shear viscosity of the 5 and 10 wt % Vectra B950 blends is used. To calculate a capillary number, the interfacial tension σ between the TLCP and the PPE/PS (70/30) matrix in the molten state is required; σ was estimated from pendent drop measurements that are described elsewhere.[16] The interfacial tension σ was measured to be approximately 1.45 mN m^{-1}.

Taking power-law viscosity behavior into account, eq. (1) now modifies to

$$Ca_{crit} = \sqrt{3}\,\frac{R \cdot \eta_{s,0} \cdot \dot{\varepsilon}^{n-1}}{\sigma} \qquad (7)$$

Using the above numerical values, Ca_{crit} is found to be 1.7 for the 5 wt % Vectra B950 blend and 5.2 for the 10% blend. These values are somewhat higher than the results found by Grace[19] for Newtonian model liquids in equilibrium shear flows, but lower than those presented by Wu[20] for polymer melts in shear flow.

CONCLUSIONS

Model experiments in elongational flow were carried out using a blend of Vectra B950 in a matrix of PPE/PS (70/30). A transition from spherical droplets to fibrils was observed when the size of the TLCP droplet exceeded a minimum value and also when the strain rate was above a critical value. The critical capillary number for fibril formation estimated from these experiments fell between those measured for

Newtonian model liquids in elongational flow and those measured for polymer melts in shear flow. Therefore, the deformational behavior of TLCP droplets seems, at least in a first approximation, to be in reasonable agreement with existing microrheological theories for multiphase flows.

From the experimental data, the elongational viscosities of the blends were calculated as well. The elongational viscosity was found to decrease with Vectra content, observe power-law behavior, and to be three ordres of magnitude larger than the shear viscosity of the blends.

The authors are grateful to W. Bruls, M. Bulters, P. Elemans, and H. Repin of DSM Research and to Prof. H. Meijer of Eindhoven University of Technology, The Netherlands, for helpful discussions.

APPENDIX

The Trumpet-Die for Elongational Flow with a Constant Rate of Strain

A constant strain rate in the capillary requires

$$\dot{\varepsilon} = \frac{dv}{dz} = \text{constant} \tag{A.1}$$

where $\dot{\varepsilon}$ is the (elongational) strain rate; z, the coordinate in the depth direction of the capillary; and v, the average velocity of the liquid flowing through the capillary (see Fig. A.1) connected to the throughput Q via

$$Q = v\pi R^2 \tag{A.2}$$

with R the radius of the capillary. Eliminating v yields

$$\dot{\varepsilon} = \frac{Q}{\pi} \cdot \frac{d}{dz}\left(\frac{1}{R^2}\right) \rightarrow \dot{\varepsilon} = \frac{-2Q}{\pi R^3}\frac{dR}{dz} \tag{A.3}$$

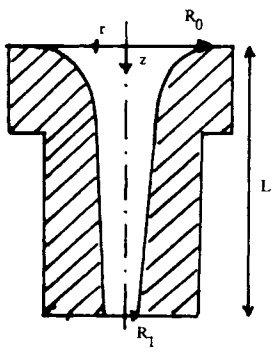

Figure A.1 Schematic view of capillary for constant elongational strain rate.

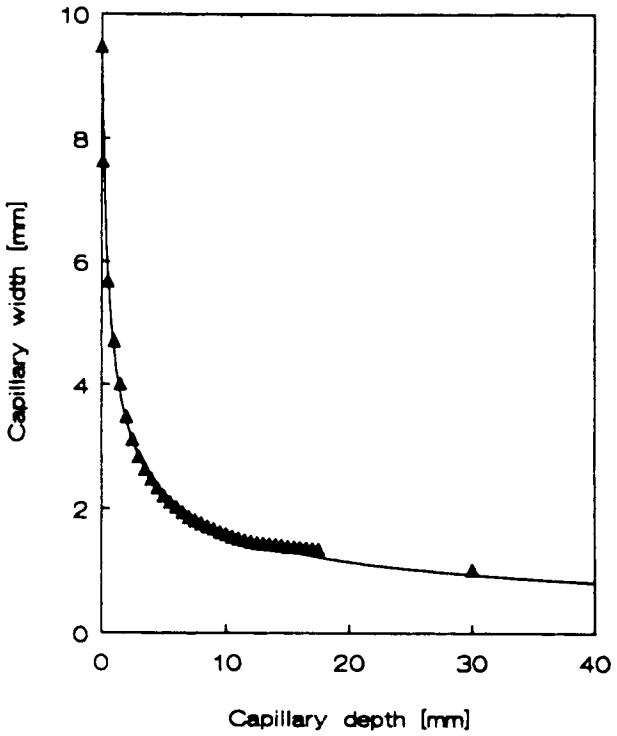

Figure A.2 Width of capillary vs. depth. Drawn line represents eq. (A.5).

or

$$\frac{\dot{\varepsilon}\pi}{-2Q}dz = \frac{1}{R^3}dR \tag{A.4}$$

Solving eq. (A.4) with the boundary condition $R = R_0$ (radius at zero depth) at $z = 0$ yields the radius of the capillary as a function of the depth:

$$R = \left(\frac{1}{R_0^2} + \frac{\dot{\varepsilon}\pi z}{Q}\right)^{-1/2} \tag{A.5}$$

with the constant

$$\frac{\dot{\varepsilon}}{Q} = \frac{1}{\pi L}\left(\frac{1}{R_1^2} - \frac{1}{R_0^2}\right) \tag{A.6}$$

relating the dimensions of the capillary (L is the capillary length) to the ratio of strain rate and throughput (or plunger speed). Figure (A.2) gives measured values of R as a function of z, as well as a graphic representation of eq. (A.5) using $\dot{\varepsilon}/Q = 1.189 \times 10^7\ \text{m}^{-3}$. From this figure, it can be concluded that an elongational deformation at constant strain rate has been realized.

Shear Contribution to the Pressure Gradient over the Capillary for Elongational Flow

Assuming a fully developed velocity profile, the pressure due to shear flow is given by

$$\frac{dP_s}{dz} = \frac{2\tau_w}{R(z)} \tag{A.7}$$

where $R(z)$ is the radius of the capillary as a function of the vertical coordinate z according to eq. (A.5) and τ_w is the shear stress at the wall. For power-law behavior [eq. (2)], τ_w is given by

$$\tau_w = \eta_0\left(\frac{Q}{\pi R(z)^3}\cdot\frac{1+3n}{n}\right) \tag{A.8}$$

Substitution into eq. (A.7) and integration over z gives

$$\Delta P_s = \int_{z=0}^{L} \frac{2\eta_0}{R(z)}\left(\frac{(1+3n)Q}{n\pi R(z)^3}\right)^n dz \tag{A.9}$$

Now eq. (A.5) can be substituted into eq. (A.9), and the integral can be rearranged to

$$\Delta P_s = 2\eta_0\left(\frac{(1+3n)Q}{\pi n}\right)^n \times \int_{z=0}^{L}\left(\frac{1}{R_0^2}+\frac{\dot{\varepsilon}\pi z}{Q}\right)^{(3n+1)/2} dz \tag{A.10}$$

Note that, because of the shape of the capillary, $\dot{\varepsilon}$ is constant and R is the only variable that depends on z. Integration yields

$$\Delta P_s = 2\eta_0\left(\frac{1+3n}{n}\cdot\frac{Q}{\pi}\right)^n\cdot\left[\frac{2Q}{3\pi\dot{\varepsilon}(n+1)}\right] \times\left[\left(\frac{1}{R_0^2}+\frac{\dot{\varepsilon}\pi L}{Q}\right)^{3(n+1)/2}-\left(\frac{1}{R_0^2}\right)^{3(n+1)/2}\right] \tag{A.11}$$

Substitution of eq. (A.6) into this result yields eq. (3).

Elongational Contribution to the Pressure Gradient over the Capillary

It can be derived from the energy equation that for pure elongational flow through a contraction the pressure difference amounts to

$$\Delta P_e = \int_{z=0}^{L} \frac{\sigma\dot{\varepsilon}}{v}\, dz \tag{A.12}$$

where the velocity v is given by

$$v(z) = \frac{Q}{\pi R(z)^2} \tag{A.13}$$

assuming plug flow. Substitution of eq. (A.5) and (A.13) into (A.12) gives

$$\Delta P_e = \int_{z=0}^{L} \frac{\eta_e\dot{\varepsilon}^2}{Q/(\pi R_0^2)+\dot{\varepsilon}z}\, dz \tag{A.14}$$

Integration now yields

$$\Delta P_e = \eta_e\dot{\varepsilon}\cdot\ln\left[\frac{Q/(\pi R_0^2)+\dot{\varepsilon}L}{Q/\pi R_0^2}\right] \tag{A.15}$$

Combination with eq. (A.13) gives eq. (4). The data in Table I, however, have been calculated using eq. (A.15) with $\dot{\varepsilon}/Q = 1.189\times10^3$ instead of eq. (4), because eq. (A.15) uses the average (measured) value of $\dot{\varepsilon}/Q$ over the entire capillary, whereas in eq. (4), $\dot{\varepsilon}$ is based only on the measured values of L, R_0, and R_1. Therefore, slightly different values for η_e are obtained if eq. (4) is used.

REFERENCES

1. G. Kiss, *Polym. Eng. Sci.*, **27,** 410 (1987).
2. W. Brostow, *Polymer,* **31,** 979 (1990).
3. P. D. Frayer, *Polym. Comp.*, **8,** 379 (1987).
4. D. G. Baird and R. Ramanathan, in *Contemporary Topics in Polymer Science, Vol. 6: Multiphase Macromolecular Systems,* B. M. Culberton, Ed., Plenum, New York, 1989.
5. D. Dutta, H. Fruitwala, A. Kohli, and R. A. Weiss, *Polym. EnHx Sci.*, **30,** 1005 (1990).
6. D. J. Williams, *Adv. Polym. Techn.*, **10,** 173 (1990).
7. G. Crevecoeur and G. Groeninckx, *Bull. Soc. Chim. Belg.*, **99,** 1031 (1990).
8. M. R. Nobile, D. Acierno, L. Incarnato, E. Amendola, L. Nicolais, and C. Carfagna, *J. Appl. Polym. Sci.*, **41,** 2723 (1990).
9. A. Valenza, F. P. La Mantia, M. Paci, and P. L. Magagnini, *Int. Polym. Proc.*, **3,** 247 (1991).
10. A. Mehta and A. I. Isayev, *Polym. Eng. Sci.*, **31,** 971 (1991).
11. A. I. Isayev and P. R. Subramanian, *Polym. Eng. Sci.*, **32,** 85 (1992).
12. G. Crevecoeur and G. Groeninckx, *Polym. Comp.*, **13,** 244 (1992).
13. G. Crevecoeur and G. Groeninckx, *Polym. Eng. Sci.*, **30,** 532 (1990).
14. G. Crevecoeur and G. Groeninckx, in *Integration of Fundamental Polymer Science and Technology-5,* P. J. Lemstra and L. A. Kleintjes, Eds., Elsevier, London, 1991.
15. G. Crevecoeur and G. Groeninckx, *Polym. Eng. Sci.*, to appear.
16. G. Crevecoeur, PhD Thesis, Catholic University of Leuven, Belgium, 1991.
17. P. H. M. Elemans, PhD Thesis, Eindhoven University of Technology, The Netherlands, 1989.

18. C. D. Han, *Multiphase Flow in Polymer Processing,* Academic Press, New York, London, 1981.
19. H. P. Grace, *Chem. Eng. Commun.,* **14,** 225 (1983).
20. S. Wu, *Polym. Eng. Sci.,* **27,** 335 (1987).
21. J. Janssen, Graduate Thesis, Eindhoven University of Technology, 1989.
22. S. Kenig, *Polym. Eng. Sci.,* **27,** 887 (1987).
23. S. Kenig, *Polym. Eng. Sci.,* **29,** 1136 (1989).
24. M. Bulters, DSM Research, Private communication.
25. F. N. Cogswell, *Polym. Eng. Sci.,* **12,** 64 (1972).
26. D. G. Baird, A. Gotsis, and G. Viola, *Polym. Sci. Technol.,* **28,** 183 (1985).
27. G. R. Mitchell and A. H. Windle, in *Development in Crystalline Polymers-2,* D. C. Basset, Ed., Elsevier, London, 1988, p. 115.
28. F. J. Baltá-Callega and C. G. Vonk, in *Polymer Science Library 8: X-Ray Scattering of Synthetic Polymers,* A. D. Jenkins, Ed., Elsevier, Amsterdam, 1989.
29. G. V. Vinogradov, N. P. Krasnikova, V. E. Dreval, E. V. Kotova, E. P. Plotnikova, and Z. Pelzbauer, *Int. J. Polym. Mater.,* **9,** 187 (1982).
30. M. P. Zabugina, E. P. Plotnikova, G. V. Vinogradov, and V. E. Dreval, *Int. J. Polym. Mater.,* **10,** 1 (1983).
31. M. V. Tsebrenko, *Int. J. Polym. Mater.,* **10,** 83 (1983).
32. S. H. Jung and S. C. Kim, *Polym. J.,* **20,** 73 (1988).
33. S. K. Bhattacharya, A. Tendolkar, and A. Misra, *Mol. Cryst. Liq. Cryst.,* **153,** 501 (1987).
34. S. K. Sharma, A. Tendolkar, and A. Misra, *Mol. Cryst. Liq. Cryst. Incl. Nonlin. Opt.,* **157,** 597 (1988).
35. C. U. Ko and G. L. Wilkes, *J. Appl. Polym. Sci.,* **37,** 3063 (1989).
36. S. M. Hong, B. C. Kim, K. U. Kim, and I. J. Chung, *Polym. J.,* **23,** 1347 (1991).
37. A. Siegmann, A. Dagan, and S. Kenig, *Polymer,* **26,** 1325 (1985).
38. G. Blizard and D. G. Baird, *Polym. Eng. Sci.,* **27,** 653 (1987).
39. F. P. La Mantia, A. Valenza, M. Paci, and P. L. Magagnini, *Rheol. Acta,* **28,** 417 (1989).
40. P. R. Subramanian and A. I. Isayev, *Polymer,* **32,** 1961 (1991).
41. F. P. La Mantia, A. Valenza, and P. L. Magagnini, *J. Appl. Polym. Sci.,* **44,** 1257 (1992).
42. D. Beery, S. Kenig, A. Siegmann, and M. Narkis, *Polym. Eng. Sci.,* **32,** 14 (1992).
43. W. L. Olbricht, J. M. Rallison, and L. G. Leal, *J. Non-Newt. Fluid. Mech.,* **10,** 291 (1982).
44. H. Giesekus, *Rheol. Acta,* **2,** 112 (1962).
45. R. J. Tanner, *AICHE J.,* **22,** 910 (1976).
46. G. G. Fuller and L. G. Leal, *J. Polym. Sci. Polym. Phys. Ed.,* **19,** 557 (1981).
47. H. E. H. Meijer and J. H. M. Janssen, in *Mixing and Compounding—Theory and Practice,* I. Manas-Zloczower and Z. Tadmor, Eds., to appear.

Received July 22, 1992
Accepted November 17, 1992